XLVI CILAMCE
VITÓRIA - ES - BRAZIL - 2025
XLVI IBERO-LATIN AMERICAN CONGRESS ON COMPUTIONAL METHODS IN ENGENEERING

Nonlinear Shallow Water Wave Propagation in a Variable-Depth Channel

Renan A. Peres[1], Antônio M. F. Frasson[1], Carlos F. Loeffler[2], Fábio P. Piccoli[1], Julio T. A. Chacaltana[1]

[1] *Postgraduate Program in Environmental Engineering, Federal University of Espírito Santo*
Avenida Fernando Ferrari, 514,Goiabeiras, 29075-910, Espírito Santo, Brazil
renan.peres@edu.ufes.br, antonio.frasson@ufes.br, fabio.p.piccoli@gmail.com, julio.chacaltana@ufes.br
[2] *Postgraduate Program in Mechanical Engineering, Federal University of Espírito Santo*
Avenida Fernando Ferrari, 514, Goiabeiras, 29075-910, Espírito Santo, Brazil
loefflercarlos@gmail.com

Abstract. The nonlinear Shallow Water Equations (SWE) for a homogeneous fluid (see, e.g., Wu *et al.* [1], Struve *et al.* [2]) is solved numerically by the Finite Element Method (FEM). Advective, hydrostatic pressure, atmospheric pressure and viscosity effects are included in the numerical solution. The baroclinic effect, Coriolis force and the wind action are disregarded in this simulation. To minimize the residual in each element, the Weighted Residuals (Galerkin) Method is used. The reflective (natural) boundary condition was implemented in order to simulate the rigid wall on right side of the channel (tank). The numerical code is written in Fortran 95 language and the Octave graphical interface is used to analyze the results. The GMSH mesh generator (v. 4.8.4) is used to represent the continuous domain by a set of discrete points that are grouped to form a non-uniform mesh of triangular elements. The numerical results of wave generation by a piston-type wavemaker (Goring [3], Whitham [4]) are compared with experimental results (Briggs *et al.* [5]) for the generation of solitary waves in a variable depth channel. The numerical results are in good agreement with those reported in the literature (Teles da Silva *et al.* [6], Takagi [7], Gardarsson [8]).

Keywords: Nonlinear; Shallow Water Equations; Finite Element Method; Solitary wave.

1 Introduction

The understanding of solitary wave propagation in shallow water through numerical methods has frequently been the focus of numerous studies, including problems related to wave generation using piston-type wavemakers (Goring [3], Francis *et al.* [9], Park *et al.* [10], Katell *et al.* [11], Song *et al.* [12]). The development of numerical models capable of accurately reproducing the nonlinear characteristics of solitary waves and their transformations due to bottom topography changes is of great importance for the understanding and prediction of natural phenomena, such as tsunamis and their interaction with coastal regions.

In this context, the present study aimed to numerically solve the nonlinear Shallow Water Equations (SWE) for a solitary wave generated by a piston-type wavemaker in a homogeneous fluid. For this purpose, the Finite Element Method (FEM) combined with the Weighted Residuals Method (Petrov-Galerkin) was employed. The simulated scenario consisted of a 23.23m x 0.5m channel with variable bathymetry (Fig. 1), based on the experimental setup presented by Briggs *et al.* [6]. Also, two approximations to the SWE — partially linear and linear — were implemented. Results were compared with those of the literature (Briggs *et al.* [5], Teles da Silva *et al.* [6], Takagi [7], Gardarsson [8]). The agreement between results proved to be promising, especially for the partially linear approximation. The behavior of the nonlinear SWE were discussed.

2 Nonlinear Shallow Water Wave Equations

The non-conservative form of nonlinear SWE are derived from the vertical integration of the mass and *momentum* equations for a Newtonian and incompressible fluid (Kanayama *et al.* [13]). This set of equations

(Eqs. 1, 2, 3) calculates the water surface elevation η from the depth of still water h, as well as the depth-averaged horizontal velocity components U and V. The model accounts for the effects of advection, hydrostatic pressure, atmospheric pressure, bottom friction and internal shear (viscosity) (Wu *et al.* [1], Struve *et al.* [2]).

$$\frac{\partial \eta}{\partial t}+\frac{\partial (HU)}{\partial x}+\frac{\partial (HV)}{\partial y}=0 \tag{1}$$

$$\frac{\partial U}{\partial t}+U\frac{\partial (U\beta_{xx})}{\partial x}+V\frac{\partial (U\beta_{xy})}{\partial y}=-g\frac{\partial \eta}{\partial x}-g\frac{\partial}{\partial x}(\frac{P_s}{g\rho_0})-Ug\frac{\sqrt{(UH^2)+(VH)^2}}{H^2C^2}+\frac{\upsilon}{H}\nabla^2(UH) \tag{2}$$

$$\frac{\partial V}{\partial t}+U\frac{\partial (V\beta_{yx})}{\partial x}+V\frac{\partial (V\beta_{yy})}{\partial y}=-g\frac{\partial \eta}{\partial y}-g\frac{\partial}{\partial y}(\frac{P_s}{g\rho_0})-Vg\frac{\sqrt{(UH^2)+(VH)^2}}{H^2C^2}+\frac{\upsilon}{H}\nabla^2(VH) \tag{3}$$

Where H $(\eta+h)$ is the total water level, β is the *momentum* correction factor (taken as 1 for the tests presented in this study), g is the gravitational acceleration, P_s is the atmospheric pressure, ρ_0 is the water density, C is the Chezy coefficient and υ is the kinematic turbulent viscosity coefficient.

2.1 Initial and Boundary Conditions

In unsteady problems described by differential equations, it is necessary to define initial conditions. In this case, an initial condition for each variable was required at a given time t_0: η_0, U_0, V_0.

$$\eta(x,y,t_0)=\eta_0=0 \quad / \quad U(x,y,t_0)=U_0=0 \quad / \quad V(x,y,t_0)=V_0=0 \tag{4}$$

Due to the spatial variation of the variables, boundary conditions are also required to solve the problem. The Dirichlet condition was applied to the U component of velocity. At the left boundary (piston-type wavemaker), the fluid velocity at the surface in contact with the piston was defined as equal to the piston velocity (Eq. 5). At the right boundary, a rigid wall was assumed, *i.e.*, $U = 0$. To ensure the numerical stability of the channel, the V component of velocity was set to zero throughout the entire 2D domain.

2.2 Solitary Wave generated by piston type wavemaker

To generate the solitary wave, the analytical expression (Eq. 5) presented by Whitham [4] was used to define the piston velocity u_p, and consequently, the velocity of the fluid particles in contact with the piston. Therefore, the piston position S_p over time could be calculated (Eq. 6), and the moving boundary was defined. Where u_0 is the maximum velocity value, C is the integration constant and $u = 1 + u_0/2$.

$$u_p=u_0\,sech^2(\sqrt{\frac{3u_0}{4}}(x-ut)) \tag{5}$$

$$S_p=-\frac{4u_0}{\sqrt{3u_0}(2+u_0)}\tanh(\sqrt{\frac{3u_0}{4}}(x-ut))+C \tag{6}$$

2.3 Stability Criterion: the Courant Number

To establish a numerical stabilization parameter, the concept of CFL stability initially proposed by Courant *et al.* [14] was adopted. This condition is currently known as the Courant Number (Eq. 7) and must be considered for both a base flow velocity $|U|$ and a wave speed c (Pulliam *et al.* [15]).

$$C_n=\frac{(|U|+c)\Delta t}{\Delta x} \tag{7}$$

3 Finite Element Method

To discretize Equations (1), (2) and (3), the Weighted Residual Method (Galerkin) was first applied. This method consists of applying a weighting function *w* to both sides of the equation in order to nullify the residual produced by an approximate solution. Subsequently, integration over the entire domain *s* was performed.

$$\int_s w\frac{\partial \eta}{\partial t}ds+\int_s w\frac{\partial (HU)}{\partial x}ds+\int_s w\frac{\partial (HV)}{\partial y}ds=0 \tag{8}$$

$$\int_s w\frac{\partial U}{\partial t}ds+\int_s wU\frac{\partial (U\beta_{xx})}{\partial x}ds+\int_s wV\frac{\partial (U\beta_{xy})}{\partial y}ds=-\int_s wg\frac{\partial \eta}{\partial x}ds-\int_s wg\frac{\partial}{\partial x}(\frac{P_s}{g\rho_0})ds-\int_s wUg\frac{\sqrt{(UH^2)+(VH)^2}}{H^2C^2}ds+\int_s w\frac{\upsilon}{H}\nabla^2(UH)ds \tag{9}$$

$$\int_s w\frac{\partial V}{\partial t}ds+\int_s wU\frac{\partial (V\beta_{xx})}{\partial x}ds+\int_s wV\frac{\partial (V\beta_{xy})}{\partial y}ds=-\int_s wg\frac{\partial \eta}{\partial y}ds-\int_s wg\frac{\partial}{\partial y}(\frac{P_s}{g\rho_0})ds-\int_s wVg\frac{\sqrt{(UH^2)+(VH)^2}}{H^2C^2}ds+\int_s w\frac{\upsilon}{H}\nabla^2(VH)ds \tag{10}$$

The Finite Element Method (FEM) was applied and the transformation from the coordinate system *s (x, y)* to the reference domain *Ω (ξ, α)* was performed (*ds = D dΩ*), where J_{nm} are the components of the Jacobian matrix and *D* is its determinant. Thus, the discrete form of the nonlinear SWE was obtained (Eqs. 13, 14, 15). The time derivative was discretized using the explicit Finite Difference Method.

$$\eta=\sum_{j=1}^{n}\eta_j N_J \;/\; HU=\sum_{j=1}^{n}HU_j N_J \;/\; HV=\sum_{j=1}^{n}HV_j N_J \;/\; U=\sum_{j=1}^{n}U_j N_J \;/\; V=\sum_{j=1}^{n}V_j N_J \;/\; w=N_i \tag{11}$$

$$\frac{\partial N}{\partial x}=\frac{1}{D}(J_{22}\frac{\partial N}{\partial \xi}-J_{12}\frac{\partial N}{\partial \alpha})=\frac{1}{D}X \quad / \quad \frac{\partial N}{\partial y}=\frac{1}{D}(-J_{21}\frac{\partial N}{\partial \xi}+J_{11}\frac{\partial N}{\partial \alpha})=\frac{1}{D}Y \tag{12}$$

$$\frac{\partial}{\partial t}\{\eta_j\}\int_\Omega N_i N_j D\,d\Omega+\{HU_j\}\int_\Omega N_i\frac{X}{D}D\,d\Omega+\{HV_j\}\int_\Omega N_i\frac{Y}{D}D\,d\Omega=0 \tag{13}$$

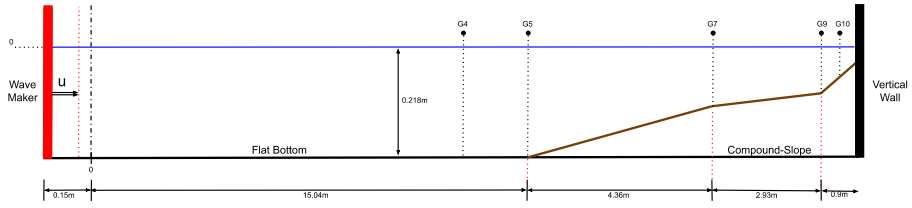
$$\begin{aligned}\frac{\partial}{\partial t}\{U\}\int_\Omega N_i N_j D\,d\Omega+\{U\}\int_\Omega U N_i\frac{X}{D}\beta_{xx}D\,d\Omega+\{U\}\int_\Omega V N_i\frac{Y}{D}\beta_{xy}D\,d\Omega=-\{\eta\}\int_\Omega gN_i\frac{X}{D}D\,d\Omega-\{\frac{P_s}{g\rho_0}\}\int_\Omega gN_i\frac{X}{D}D\,d\Omega\\ -\{U\}\int_\Omega N_i N_j\theta g\frac{\sqrt{(UH^2)+(VH)^2}}{H^2C^2}D\,d\Omega+[\oint w\frac{\upsilon}{H}\nabla(UH).\hat{\boldsymbol{n}}dl-\{U\}\int_\Omega\frac{\upsilon}{H}\nabla N_i.\nabla(N_jH)D\,d\Omega]\end{aligned} \tag{14}$$

$$\begin{aligned}\frac{\partial}{\partial t}\{V\}\int_s N_i N_j ds+\{V\}\int_s U N_i\frac{\partial N_j}{\partial x}\beta_{yx}ds+\{V\}\int_s V N_i\frac{\partial N_j}{\partial y}\beta_{yy}ds=-\{\eta\}\int_s gN_i\frac{\partial N_j}{\partial y}ds-\{\frac{P_s}{g\rho_0}\}\int_s gN_i\frac{\partial N_j}{\partial y}ds\\ -\{V\}\int_s N_i N_j\theta g\frac{\sqrt{(UH^2)+(VH)^2}}{H^2C^2}ds+[\oint w\frac{\upsilon}{H}\nabla(VH).\hat{\boldsymbol{n}}dl-\{V\}\int_s\frac{\upsilon}{H}\nabla N_i.\nabla(N_jH)ds]\end{aligned} \tag{15}$$

4 Test Case

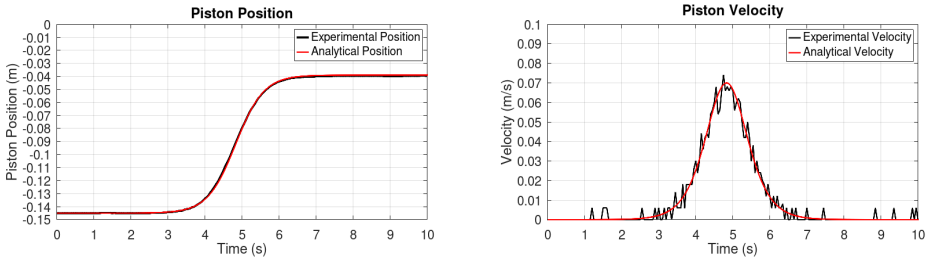
The simulated case is presented as Case A of Problem 3 from a series of experiments conducted by Briggs *et al.* [5]. It involves an experiment on solitary wave generation using a piston-type wavemaker. For this purpose, a tank measuring 23.23m in length and 0.5m in width was used, with variable bathymetry starting at 15.04m (Fig. 1). The piston began its motion at approximately -0.15m and reached $u_0 = 0.07$m/s at $t \sim 4.8$s.

Figure 1. Test case.



Water surface elevation was recorded at Stations G4, G5, G7, G9 and G10 and at the vertical wall. Equations (5) and (6) were calibrated for flow generation based on the experimental data (Fig. 2).

Figure 2. Piston velocity and position.



The depth of still water (h) of the flat bottom section is 0.218m. The depth and position along the x-axis of the other stations are presented in Table 1. It is important to note that the long-wave condition was respected.

Table 1. Parameters of mesh, wave properties and stations positions.

Width (m)	**Length (m)**	**Δx (m)**	**Δt (s)**
0.5	23.3	0.05	0.005
Wave Period (s)	**Wave-length (m)**	**c_{wave} Maximum (m/s)**	**Courant Number**
~ 6	~ 8.94	1.49	0.149
Station	**X coordinate (m)**	**Y coordinate (m)**	**Depth h (m)**
G4	12.64	0.25	0.218
G5	15.04	0.25	0.218
G7	19.40	0.25	0.136
G9	22.33	0.25	0.116
G10	22.80	0.25	0.080

Next, some of the results obtained for the nonlinear, partially linear and linear equations are discussed. The nonlinear equation refers to the full equation as presented (Eqs. 8, 9, and 10). In the linear equation, the wave speed c and the advective term were linearized. To eliminate the dispersive effect of the advective term, the base flow velocity U_0 and the wave-induced velocity U_1 were considered. This approximation, derived from perturbation theory (Eq. 16), allows the linearization of the advective term in the shallow water equations by considering only the order zero (ε_0) and first-order (ε_1) solutions, as adopted in various studies (Kanayama [16], Huang *et al.* [17], Subich [18], Lilly *et al.* [19]). However, since there is no base flow ($U_0 = 0$) in the present experiment, both the order zero and first-order solutions are null.

$$(\vec{U}.\nabla)\vec{U} = \varepsilon_0(\vec{U}_0.\nabla)\vec{U}_0 + \varepsilon_1[(\vec{U}_1.\nabla)\vec{U}_0 + (\vec{U}_0.\nabla)\vec{U}_1] \tag{16}$$

To linearize the wave speed c, the maximum elevation value η_{max} was assumed within the Newton binomial expansion (Eq. 17), as proposed by Whitham [3]. Only the order zero and first-order terms were considered. In the partially linear equation, only the linearized wave speed c was taken into account.

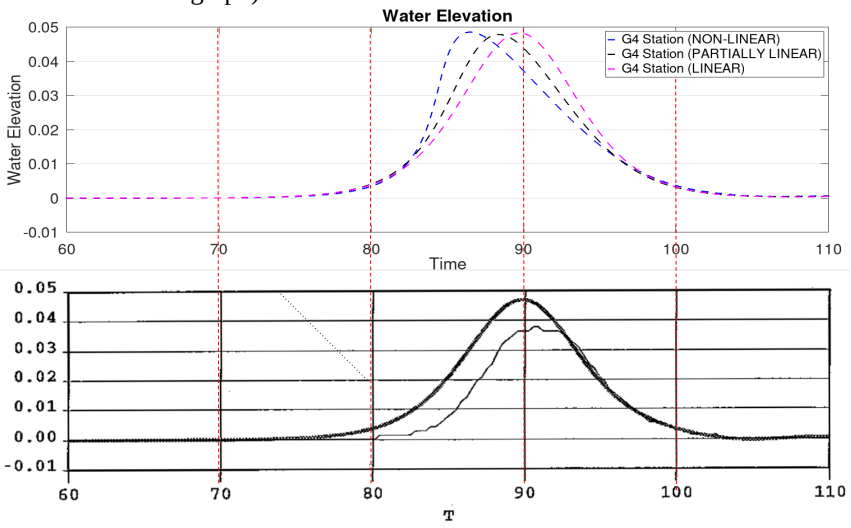
$$c \approx \sqrt{gh}\left(1 + \frac{1}{2}\frac{\eta_{max}}{h} - \frac{1}{8}\left(\frac{\eta_{max}}{h}\right)^2 + \frac{1}{16}\left(\frac{\eta_{max}}{h}\right)^3 - \ldots\right) \tag{17}$$

The first analysis concerns the water surface elevation at Station G4 and at the vertical wall, considering the experimental results by Briggs *et al.* [5] and the numerical results obtained by Teles da Silva *et al.* [6]. Next, an analysis of the spatial evolution of the wave was performed, and the results were compared with those reported by Takagi [7]. Finally, measurements at all stations were recorded and analyzed in relation to both the experimental data and the numerical results presented by Gardarsson [8].

5 Results and Discussion

In the first analysis, it was possible to identify the dispersive effect of the nonlinear SWE present in the nonlinearity of the advective term and the wave speed c. By recording the water surface elevation at Station G4, the tendency for wave steepening was observed, as the wave peak travels at a higher velocity. This effect is completely eliminated in the linear approximation. However, in the partially linear approximation the nonlinear advective effect still contributes to the wave steepening (Fig. 3).

Figure 3. Water surface elevation results at Station G4 for the nonlinear (blue), partially linear (black) and linear solution (purple). Experimental results (thin line - second graph) and numerical results obtained by Teles da Silva *et al.* [6] (thick line - second graph).



The simulated maximum water surface elevation values were very close to the estimated ones for all solution types at Station G4 and at the wall (Table 2). The exception was the nonlinear solution, which, due to relatively rapid wave steepening, collapsed before reaching the wall. Regarding the wave arrival time at Station G4, all solutions were close to the expected value (around t = 80), especially the linear approximation.

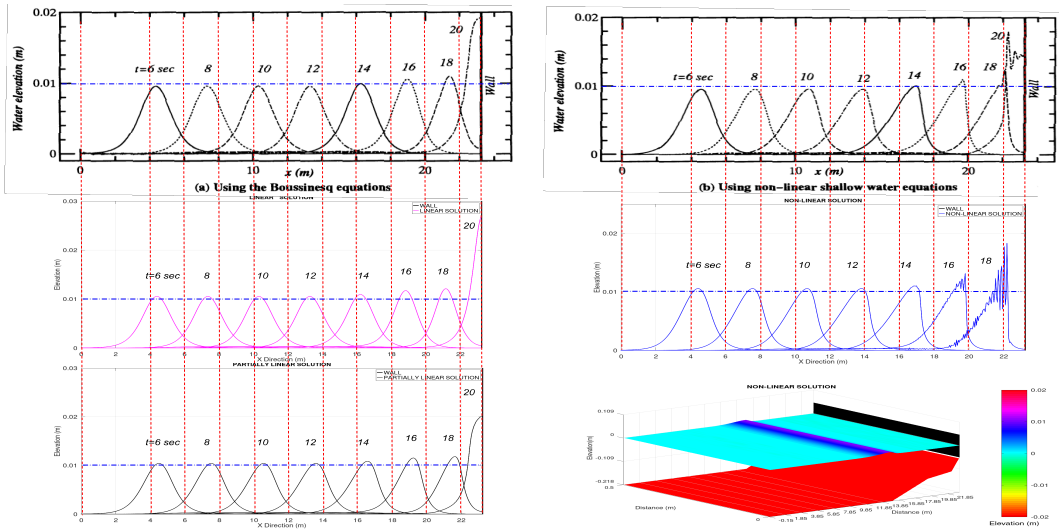
Table 2. Elevation values at Station G4 and on the vertical wall.

Measuring point	***Estimated*** η_{max} **(m)**	***Simulated*** η_{max} **(m) - Nonlinear -**	***Simulated*** η_{max} **(m) - Partially Linear -**	***Simulated*** η_{max} **(m) - Linear -**
Station G4	0.0109	0.0105	0.0104	0.0105
Wall (Runup)	0.0274	--	0.0269	0.0268

In the second analysis, the spatial propagation of the nonlinear solution and partially linear and linear approximations was analyzed at time instants 6s, 8s, 10s, 12s, 14s, 16s, 18s and 20s. The results obtained (Fig. 4) were very close to the numerical results reported by Takagi [7]. This analysis showed that the partially linear and linear approximations closely matched the Boussinesq solution, while the nonlinear solution was consistent with Takagi's own nonlinear SWE solution [7]. In this result, the wave tended to steepen and break around t=16s.

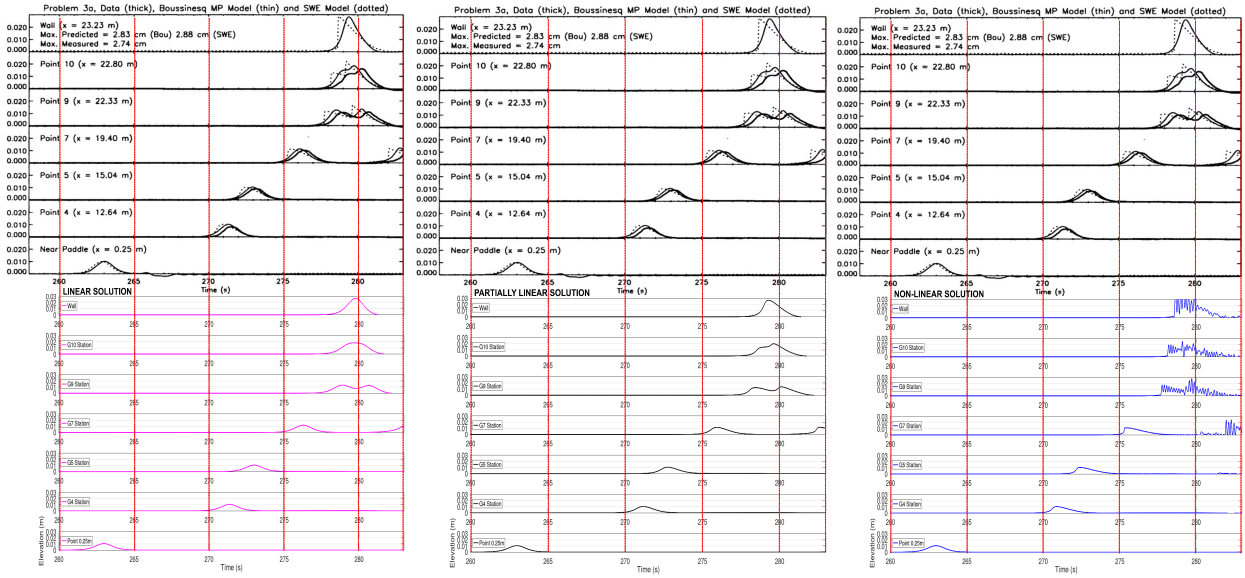
A slight delay in the arrival of the linear wave at the wall compared to the Boussinesq solution presented by Takagi [7] was identified. This difference is believed to be due to the approximations adopted in linearizing the nonlinear SWE, since these approximations disregarded the advective effect. In contrast, the partially linear approximation was the closest to the Boussinesq solution. Although wave steepening was still present, it exhibited a close behavior at the wall at t=20s, including the water elevation value.

Figure 4. Water surface elevation of the nonlinear (blue), partially linear (black) and linear solution (purple). Numerical results by Takagi [7] from the nonlinear SWE (top left) and the Boussinesq equations (top right).



Finally, the water surface elevation results at all stations and the vertical wall are presented (Fig. 5). For this purpose, a simulation time of 25s was used, which was sufficient for the wave to reflect off the wall and its return to be detected at Stations G7, G9 and G10. As observed in previous simulations, the nonlinear solution led to wave steepening and breaking around 16s, causing the model to collapse after this instant. The results were compared with experimental data and numerical results obtained by Gardarsson [8] (SWE and Boussinesq equations). Once again, the partially linear approximation was the closest to the experimental data, capturing the asymmetry present at Stations G9 and G10, thereby better approximating reality. It can be concluded that this effect results from the nonlinearity of the advective term, highlighting its relevance for a more faithful representation of reality. It was verified that in the absence of this effect, the asymmetry is lost, as seen in the linear approximation. Therefore, although the linear approximation provides good results regarding wave arrival time and amplitude, certain peculiarities, such as asymmetry, cannot be reproduced by linear effects.

Figure 5. Water surface elevation of the nonlinear (blue), partially linear (black) and linear solution (purple) at all stations. Numerical results obtained by Gardarsson [8] (top graph).



6 Conclusions

The numerical experiments conducted in this study revealed that the nonlinear shallow water model does not preserve the shape of the solitary wave during its propagation, underscoring the model's limitations for the

present case. This is mainly due to the dispersive effect present in the advective term and the wave speed *c*. In the simulated scenario - where the ratio between the maximum elevation η_{max} and the depth of still water *h* was approximately 5% - this effect resulted in wave steepening and, consequently, the collapse of the model after a certain simulation time. It is worth noting that despite the wave steepness parameter ε - $2\pi\eta_{max}/\lambda \ll 1$ - being respected, the relative wave height parameter - $2\pi\eta_{max}/h \ll 1$ - reached a value of approximately 0.4 at the wave breaking point. In this scenario, the difference between the wave velocity at the lowest points - $c=\sqrt{gh} \simeq 1.46\, m/s$ - and at the wave crest - $c=\sqrt{g(\eta_{max}+h)} \simeq 1.49\, m/s$ - was still relatively large. This caused the wave peak to travel a significant fraction of the wavelength within a few seconds, resulting in the formation of an almost vertical wave front - the moment at which the model collapses. The linear approximation showed good agreement with the water surface elevation values and wave arrival times at the stations. However, without the advective term it was unable to reproduce the asymmetries observed in the experimental results. In contrast, the partially linear approximation best approximated reality: even without considering dispersion in the wave speed *c*, the model did not collapse and was still able to accurately represent the asymmetries, which are a result of the nonlinearity present in the advective term that was retained.

Acknowledgements. The authors would like to thank the local organizing committee, the Postgraduate Program in Environmental Engineering (PPGEA) at the Federal University of Espírito Santo, and the Fundação de Amparo à Pesquisa do Estado do Espírito Santo (FAPES), the Brazilian Postgraduate Agency.

Authorship statement. The authors hereby confirm that they are the sole liable persons responsible for the authorship of this work, and that all material that has been herein included as part of the present paper is either the property (and authorship) of the authors, or has the permission of the owners to be included here.

References

[1] Wu, Y. *et al.* Mathematical modelling of tidal currents in mangrove forests. **Environmental Modelling & Software,** v. 16, p. 19–29, 2001.
[2] Struve, J. *et al.* Influence of model mangrove trees on the hydrodynamics in a flume. **Estuarine, Coastal and Shelf Science,** v. 58, p. 163–171, 2003.
[3] Goring, D. G. Tsunamis - The Propagation of Long Waves onto a Shelf. 355f. **Thesis** (PhD), Division of Engineering and Applied Science. California Institute of Technology. Pasadena, California. 1978.
[4] Whitham, G. B. **Linear and Nonlinear Waves**. John Wiley & Sons, Inc. New York. 1974.
[5] Briggs, M. J. *et al*. Runup of Solitary Waves on a Vertical Wall. *In:* **Long-Wave Runup Models**. Wolrd Scientific. Singapore. 1996.
[6] Teles da Silva, A. F. T. *et al.* Numerical Simulations of Solitary Wave Generation and Runup on a Canal Compared with Experiment. *In:* **Long-Wave Runup Models**. Wolrd Scientific. Singapore. 1996.
[7] Takagi, T. *et al.* Finite Element Analysis in Bench Mark Problems 2 and 3. *In:* **Long-Wave Runup Models**. Wolrd Scientific. Singapore. 1996.
[8] Gardarson, S. M. *et al.* Runup of Solitary Waves on a Vertical Wall. *In:* **Long-Wave Runup Models**. Wolrd Scientific. Singapore. 1996.
[9] Francis, V. *et al.* Generating stable solitary waves with a piston-type wavemaker. **Coastal Engineering,** v. 157, 2020.
[10] Park. J. *et al.* A numerical experiment on a new piston-type wavemaker: Shallow water approximation. **International Journal of Naval Architecture and Ocean Engineering**, v. 15, 2023.
[11] Katell, G. *et al.* Accuracy of solitary wave generation by a piston wave maker. **Journal of Hydraulic Research**, v. 40, n. 3, 2002.
[12] Song, X. *et al.* Numerical Generation of Solitary Wave and Its Propagation Characteristics in a Step-Type Flume. **Journal of Marine Science and Engineering**, v. 11, n. 35, 2023.
[13] Kanayama, H. *et al.* On the viscous shallow-water equations. I. Derivation and conservation laws. **Mem. Numer. Math.** no. 8-9, p. 39–64, 1982.
[14] Courant, R. *et al*. Uber die partiellen Differenzengleiehungen der mathematisehen Physik. **Mathematische Annalen**. v. 100, 1928.
[15] Pulliam, T. H. *et al.* **Fundamental Algorithms in Computational Fluid Dynamics**. Springer International Publishing Switzerland, 2014
[16] Kanayama, H. *et al.* On the viscous shallow-water equations. II. A linearized system. **Bull. Univ. Electro-Comm**. v. 1, n. 2, p. 347–355, 1988.
[17] Huang, A. *et al.* The Linearized 2D Inviscid Shallow Water Equations in a Rectangle: Boundary Conditions and Well-Posedness. **Archive for Rational Mechanics and Analysis**, 2012.
[18] Subich, C. Instabilities in the Shallow-Water System with a Semi-Lagrangian, Time-Centered Discretization. **Monthly Weather Review**, v. 150, 2022.
[19] Lilly, J. R. *et al.* CFL Optimized Forward–Backward Runge–Kutta Schemes for the Shallow-Water Equations. **Monthly Weather Review**, v. 151, 2023.